

Internal corrosion prevention in slurry pipelines using nitrogen gas: a case study

<http://dx.doi.org/10.1590/0370-44672021770002>

Ayron Silva Guimarães Torres^{1,5}

<https://orcid.org/0000-0001-7804-6867>

Vanessa de Freitas Cunha Lins^{2,6}

<https://orcid.org/0000-0002-6357-9553>

Gabriela Goes Mattioli^{3,7}

<https://orcid.org/0000-0003-3588-4697>

Paulo Roberto Gomes Brandao^{4,8}

<https://orcid.org/0000-0002-5893-1073>

¹Samarco Mineração S.A., Gerência de Mineroduto, Engenharia de Integridade de Dutos, Mariana – Minas Gerais – Brasil.

²Universidade Federal de Minas Gerais – UFMG, Escola de Engenharia, Departamento de Engenharia Química, Belo Horizonte - Minas Gerais - Brasil.

³Samarco Mineração S.A., Gerência de Mineroduto, Engenharia de Processo, Mariana - Minas Gerais – Brasil.

⁴Universidade Federal de Minas Gerais – UFMG, Escola de Engenharia, Departamento de Engenharia de Minas, Belo Horizonte - Minas Gerais - Brasil.

E-mails: ⁵ayront@gmail.com, ayron.torres@samarco.com,

⁶vlins@deq.ufmg.br, ⁷gabimattioli@hotmail.com,

gabriela.goes@samarco.com, ⁸pbrandao@demin.ufmg.br

Abstract

The transport capacity of the slurry pipelines is related to the internal roughness of the pipe. Thus, the application of corrosion protection methods is of fundamental importance, both in the operational phase and in times of temporary shutdown. In addition, corrosion also affects the service life of the duct. The studied pipeline was hibernated with nitrogen using the ABNT NBR 15280-2 standard as a reference and remained hibernated for 3.5 years. Chemical, mineralogical, and microstructural analyses were carried out on samples of materials removed from the pipeline interior during the hibernation period. The most striking phase found was magnetite, with botrioidal morphology, formed by the oxidation of steel in the pipeline. After reactivation, the pipeline was inspected by smart pigs with ultrasound and MFL technologies. It was found that the corroded regions are more concentrated in the initial kilometers of the sections, where important depths of corrosion were also observed, as well as higher rates of corrosion and erosion, which show the influence of the operational phase in the development of the pipeline corrosive process and wear. Thus, the application of the nitrogen hibernation process in long-distance pipelines proved to be feasible for long periods of time. However, improvements are suggested in this article to make the process more robust.

keywords: corrosion, pipeline, hibernation, nitrogen.

1. Introduction

Buried pipelines are subjected to external and internal corrosion. External corrosion can be corrosion induced by microorganisms (Liu *et al.*, 2021), generated by stray currents (Peng *et al.*, 2020), or induced by other aggressive factors (Liu *et al.*, 2019). Considering the internal corrosion, the transports capacity of pipelines is related to the internal pipe

roughness (Mattioli *et al.*, 2018). In this sense, the internal corrosion of the ducts plays an important role since it increases the roughness and reduces the capacity of the system, by increasing the friction factor (Taylor *et al.*, 2006; Díaz-Damacillo & Plascencia, 2019). In addition to the reduction in transport capacity, corrosion also affects the life cycle of the pipelines due to

the reduction in the wall thickness of the tubes. The potential for damage that corrosion causes to the pipeline is increased by synergism with the erosion caused by the slurry displacement (Islam & Farhat, 2017; Elemuren *et al.*, 2018; Aguirre & Walczak, 2018). At certain times during the operational phase, the temporary shutdown of a pipeline may be necessary

for legal or strategic reasons. To minimize internal corrosion in the stopped lines, two hibernation methodologies can be applied: filling the duct with water treated with inhibitors and biocides; and filling the duct with nitrogen gas (Lins *et al.*, 2016). Studies on the hibernation process in slurry pipelines that have already operated are scarce in literature. Hibernation studies with treated water before the start operations have already been carried out

2. Materials and methods

The nitrogen hibernation method was applied to the slurry pipeline. Corrosion products removed from the inside of the duct were submitted to laboratory analysis. After the nitrogen hibernation period, in-line inspections were performed with smart pigs to detect corruptions. Using the results of the smart pig inspections, it was possible to evaluate the corrosive process during the nitrogen hibernation period.

The inside of the pipeline was hibernated with injected nitrogen gas, remaining in this condition for 3.5 years. The criteria for considering a duct hibernated with nitrogen were taken from the Brazilian standard ABNT NBR 15280-2, highlighting the following items: dew point temperature in 0°C (1 atm); oxygen content less than 5%; and gas pressure larger than or equal to 49 kPa.

Material samples were removed from inside the pipeline by smart pigs, and were analyzed in order to access their chemical and mineralogical compositions. The overall sample had a particle size between 0.038 mm

(Lins *et al.*, 2016). In the case of the hibernation process with nitrogen injection, in the oil and gas industries, there are Brazilian regulations for conditioning the pipelines during the construction and assembly phase (ABNT NBR 15280-2 : 2015). Both techniques have already been applied to a mining company in Brazil. The choice of each methodology was carried out according to risk and environmental analyses. In the case of nitrogen hibernation, the

and 0.85 mm. The chemical analysis was made by the wet method through the dichromatometry technique for Fe₂O₃, while FeO; CaO, SiO₂, Al₂O₃, P and MnO₂ were analyzed by atomic emission spectroscopy with inductive coupled plasma (ICPAES). The atomic emission spectrometer used was the Ciros, CCD model. Iron contents were converted from Fe to Fe₂O₃. Loss on ignition (LOI) was determined by calcination in an oven and the consequent weight difference. Polished sections were prepared for microscopic studies, using impregnation with epoxy resin. Only diamond pastes were used in the final polishing step with loose abrasives. Samples were pulverized in a pot mill and then analyzed by X-ray diffraction and X-ray fluorescence spectrometry. The X-ray diffractometer used was Philips (Panalytical) for powder samples, with an X'Pert-APD system, PW 3710/31 controller, with a Cu anode. The X-ray fluorescence spectrometer used was Philips (Panalytical), PW 2400 model, having an Rh anode. The

choice considers that a possible leak of the gas into the environment would not result in significant environmental impacts, being the most environmentally friendly method. This article aims to present a case study on the application of nitrogen hibernation in a long-distance pipeline, with approximately 400 kilometers in length, which transports iron ore slurry. To our best knowledge, there is no report in literature on this topic.

microstructure studies were carried out by scanning electron microscopy (SEM) dual, with field emission gun (FEG) from FEI, Dual-FIB Quanta 3D model, with energy-dispersive X-ray spectrometry (EDS) from BRUKER, Nano X Flash Detector 5010 model, software Esprit. Backscattered electrons (BSE) images are always shown in this study. A very thin film of carbon was deposited on the polished samples to promote the surface's electrical conduction.

The pipeline was inspected with smart pigs assembled with ultrasound and MFL (Magnetic Flux Leakage) tools. Corrosion along the pipeline was evaluated for its distribution, the relationship of these distributions, and the pipeline elevation profile was verified. To carry out the corrosion rate calculations, the design wall thickness and the remaining wall thickness measured with smart pigs were used, since only one pig inspection was performed. The pipeline operated for 7 years before being hibernated. Thus, erosion rate calculations were also performed.

3. Results

The materials removed from the inside of the pipeline were characterized

and the results of the chemical analysis are shown in Table 1.

Table 1 - Global chemical composition of the sample (wt.%).

PPC	Fe	FeO	SiO ₂	Al ₂ O ₃	P	Mn	CaO	MgO	TiO ₂	Total
5.05	64.18	10.50	1.03	0.394	0.049	0.793	0.779	0.038	0.016	82.83

The mineralogical composition was defined with the support of the chemical composition, since it was not possible to quantify the phases identified by X-ray diffraction, since the results using the Rietveld-based method would not be reliable, due to the low degree of crystallinity of all

mineral phases. Thus, a conciliation with chemical analysis was not viable, due to insufficiency and redundancy of data. However, the estimation of the abundance of phases, compared with the respective chemical analysis, is reliable, although semiquantitative. In addition to the intensity of the peaks in the

diffractograms, the abundance of magnetite is confirmed by the clear degree of magnetism observed in macroscopic samples. Table 2 shows the results obtained by using the X-ray diffraction and X-ray fluorescence spectrometry tests in terms of quantification levels and phase abundance, respectively.

Table 2 - Results obtained in the X-ray diffraction and X-ray fluorescence spectrometry.

X-ray fluorescence spectrometry	
Elements	Global Sample
Fe, O	high
Mn, Ca, Si	medium
Al, Cr	low
P, Mg, Ti, S, Ni, Cl	traces
X-ray diffraction	
Minerals	Global Sample
magnetite	abundant
hematite	medium
goethite	medium
calcite	low

The microstructure results are of typical tubercles, showing individual differences.

Figure 1 shows three fragments of tubercles, which present a predominantly botryoidal

texture, with moderate presence of large sub-millimeter pores, but with several smaller ones.

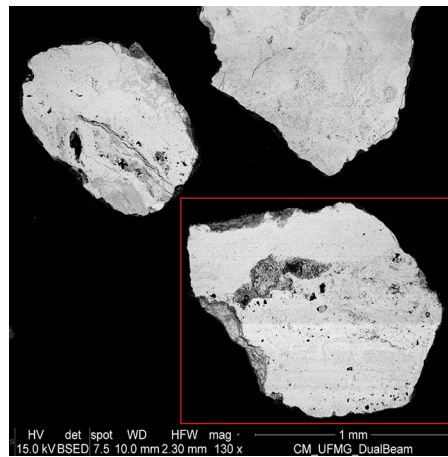


Figure 1 - Three fragments of tubercles, with approximately millimeter size.

Looking in detail at the tubercle fragment at the bottom of the image in Figure 1 (red box region), there is a clear botryoidal fabric in the median region.

Virtually all microstructural features are secondary, that is, they are products of corrosion, as can be seen in Figure 2, where Ms and Hs are respectively, regions

of magnetite and hematite, both secondary with generally botryoidal morphology, Po is the region of a pore and R is the impregnation resin.

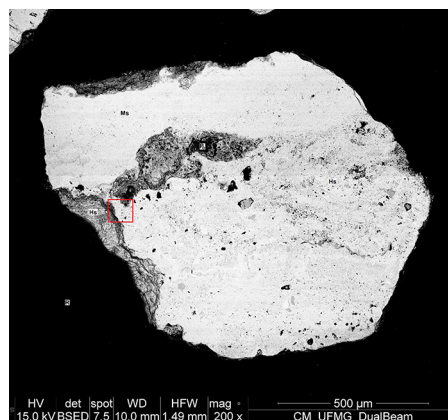


Figure 2 - Tubercle fragment with botryoidal fabric.

Applying an enlargement of the tubercle in Figure 2 (red box region),

parallel concentric bands of magnetite and hematite were identified, both sec-

ondary, as shown in Figure 3.

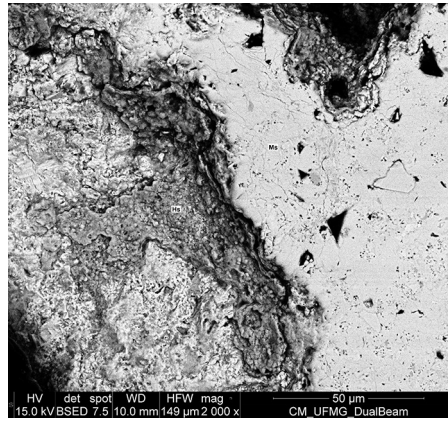


Figure 3 - Parallel bands of magnetite and hematite.

Figures 4 and 5 show details of other analyzed tubercles. Figure 4 shows bot-rioidal texture, with alternating bands of

magnetite and hematite, both secondary, with grains of goethite (Go), also. Figure 5 shows a pore, partially filled with aggregate

and containing a calcite grain (Ca). Aggregates are made up of secondary and primary particles cemented by calcite.

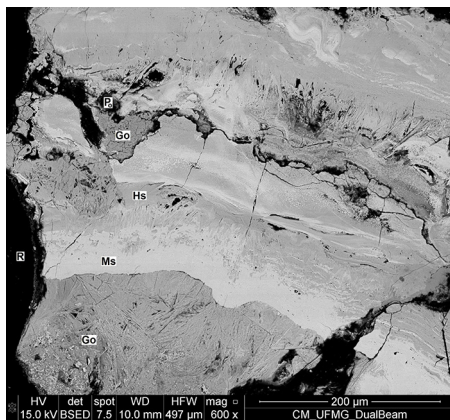


Figure 4 - Tubercle detail with goethite grains.

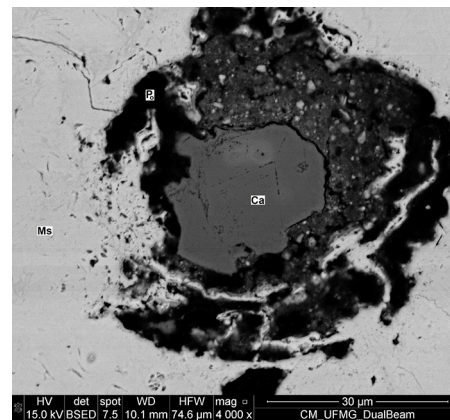


Figure 5 - Pore partially filled with aggregate and containing a calcite grain.

The analysis of the corrosion results was carried out separately for the two sections of the pipeline. In this

article, only the results for section 1 are presented, as the pattern of results was the same as that observed in section 2.

Figure 6 shows the corroded regions and the elevation profile along the pipeline length for section 1.

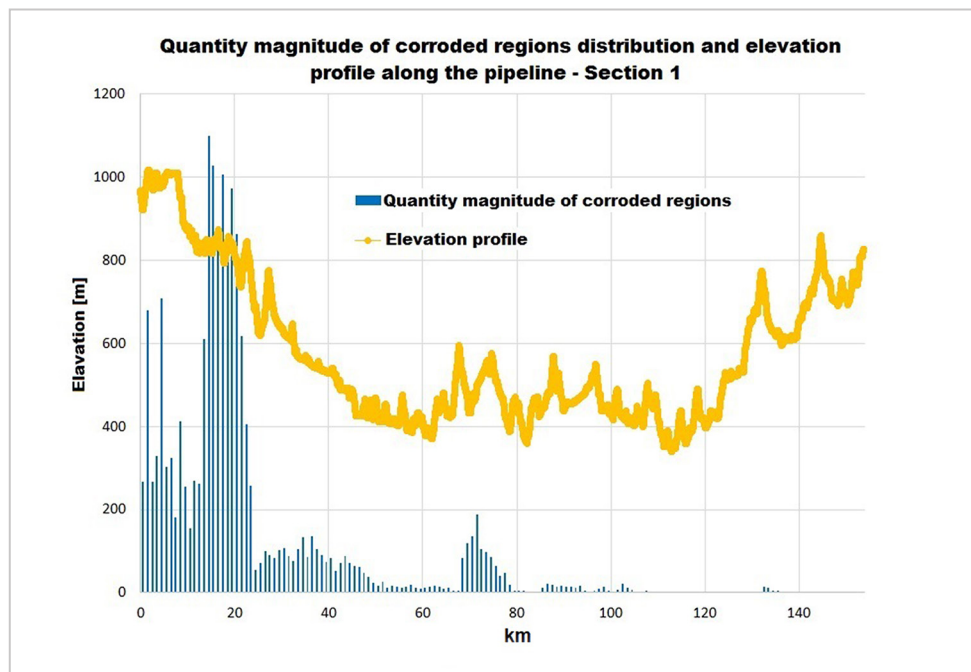


Figure 6 - Corroded regions distribution and elevation profile along the pipeline - Section 1.

Figure 7 shows the extension magnitude of corroded regions and the elevation profile along the length of the pipeline for section 1.

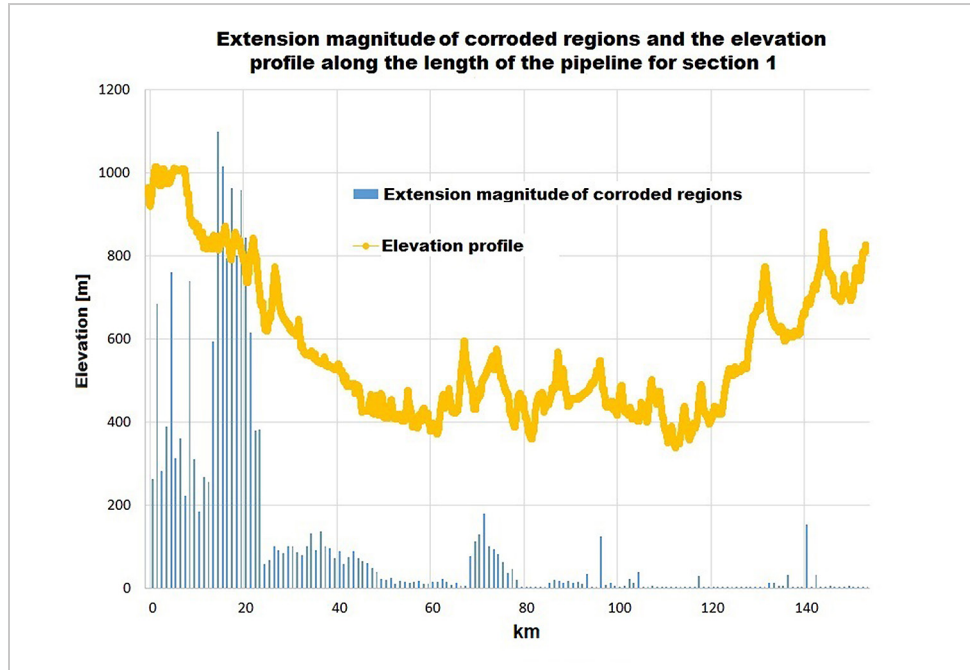


Figure 7 - Corroded regions distribution and the elevation profile along the length of the pipeline for section 1.

Figure 8 shows the o'clock positions of the corroded regions along the length of the pipeline in section 1.

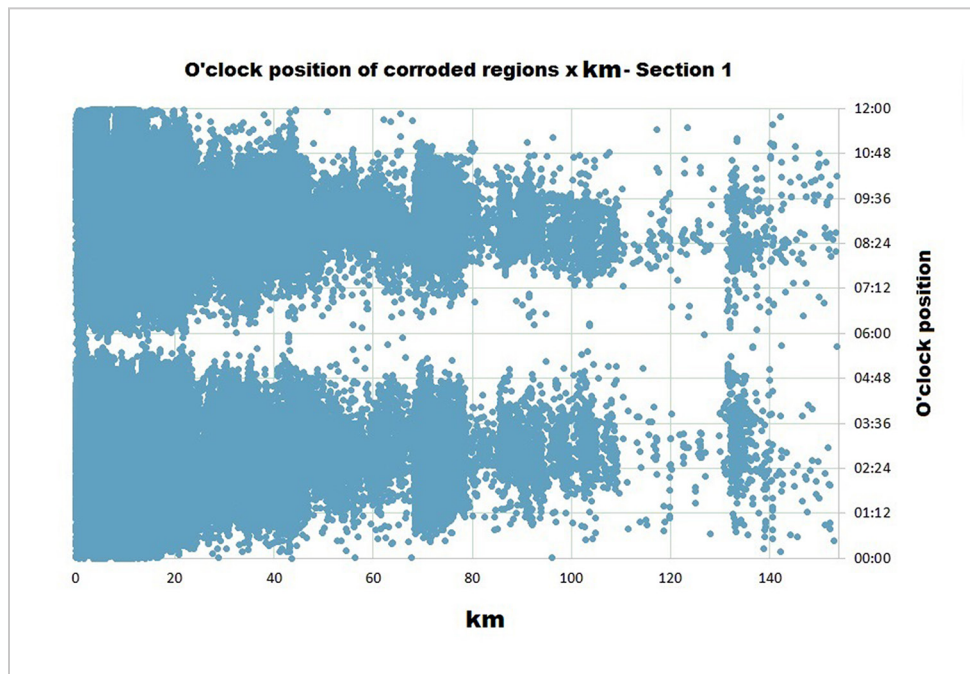


Figure 8 - O'clock positions of corroded regions along the length of the pipeline - Section 1.

The o'clock positions of 03:00, 06:00, 09:00 and 12:00 hours indicate, respectively, the right, bottom, left and top generatrices of the pipe.

Figure 9 shows the corrosion rates along the pipeline.

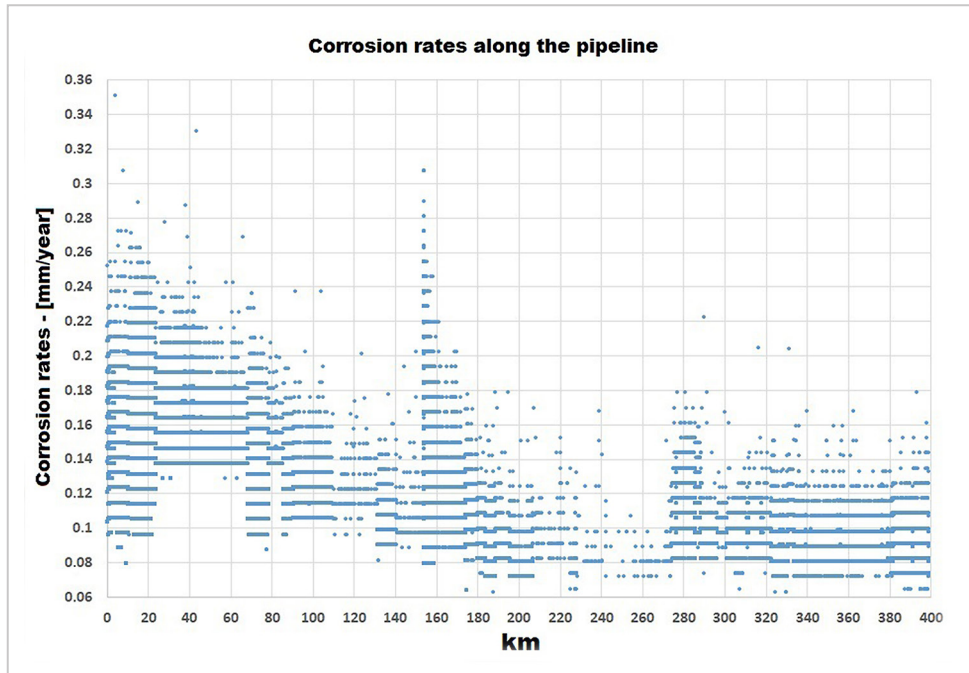


Figure 9 - Corrosion rates along the pipeline.

Figure 10 shows the erosion rates across the entire pipeline.

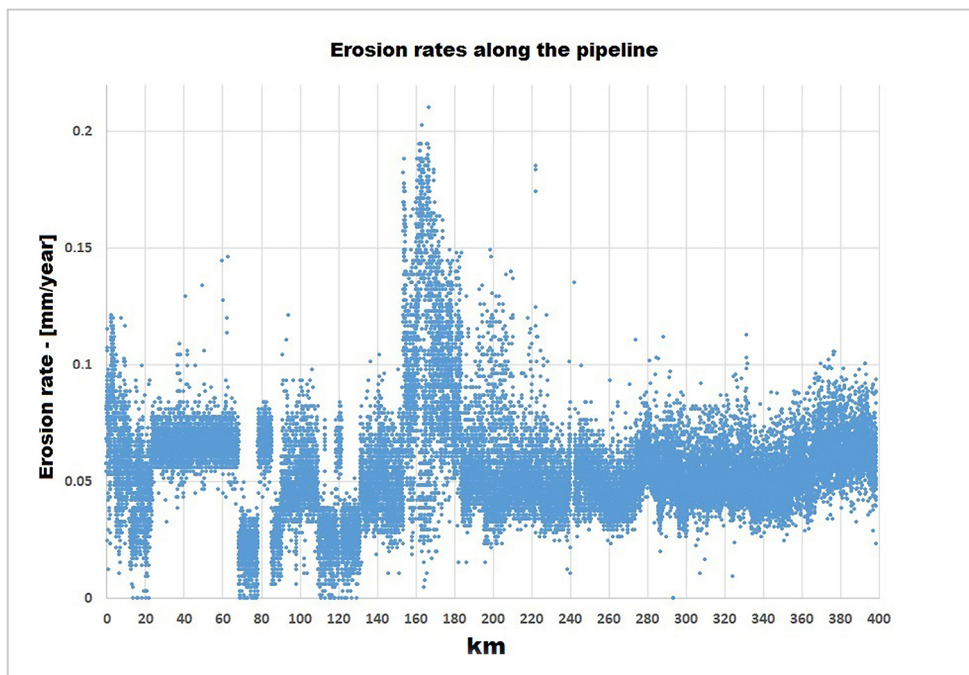


Figure 10 - Erosion rates along the pipe.

The corrosion rate calculation was performed considering the minimum wall

thicknesses found for each pipe, and the erosion rate calculation was performed

considering the most measured value of wall thickness per pipe.

4. Discussion

Using a microstructural analysis, with the support of chemical and mineralogical analyses by X-ray diffraction, it was found that the most important phase is magnetite, with botrioidal morphology, rarely massive; this phase is the main cause of the ferromagnetic property of the materials removed from the pipeline

and examined in this study. This magnetite is formed by the oxidation of steel in the pipeline tube; it should be noted that the natural magnetite, that is, originally present in the transported concentrates, is very seldomly found; thus, almost all the magnetite analyzed comes from corrosion and is called secondary. Hematite is

the second phase in abundance. A minor part of the hematite, certainly, comes from the iron ore concentrate (primary); however, in the case of the studied sample, the major fraction of the hematite has originated from the oxidation of the steel, being, therefore, secondary. Only by using microstructural analysis, mainly by

the botryoidal morphology, it is possible to distinguish primary from secondary hematite. The mineral goethite shows the same ambiguity of origin as hematite, with the complication that goethite is almost always botryoidal. The main criterion for distinction is using microstructure analysis, by the intimate occurrence of goethite in the structure of the tubercle. The calcite phase is derived entirely from the calcium hydroxide added to the concentrate. A vast majority of the studied particles are composed of tubercles; in the current sample practically all the particles studied are fragments, even in the coarsest particle size fraction. Tubercles are composed essentially of steel corrosion products and include varying amounts of fine ore and usually fine calcite, derived from calcium hydroxide carbonation.

Corroded regions are more concentrated in the initial kilometers of the sections, as presented in Figure 6, that is, after the pumping stations. A higher percentage of corroded regions was observed in the first 23 kilometers; this amount reduces but is still considerable up to 46 kilometers. At three other points, the quantities of corroded regions can be highlighted, between kilometers 68 and 78 more significantly, between 85 and 109 and between 130 and 140, in lesser quantity. In these three points, a similar behavior is observed. The erosion is in the bottom regions of the profile, which may be an indication that there was an accumulation of moisture in these places, favoring the development of corrosive processes. The extension magni-

5. Conclusions

The application of the nitrogen hibernation process in long-distance pipelines proved to be feasible for long periods of time.

Corroded regions are more concentrated in the initial kilometers of the sections, that is, after the pumping stations, highlighting the influence of the operational phase in the development of the corrosive process, due to the oxygen dissolved in the water, and not because of failures in the process of hibernation with nitrogen. Another factor that corroborates this point of view is that the greatest corrosion depth and corrosion rates, for the most part, are located in these initial kilometers.

It was not possible to establish a correlation between the corroded regions with the elevation profile of the pipe, but

tude of corroded regions along the length of the pipeline was analyzed.

The analysis of the results presented in Figure 7 showed that the extension of the corroded regions, as expected, was higher where there are higher densities of corroded regions. However, it was possible to observe that, in certain kilometers, even with a low density of corroded regions, the extension of the corroded region was higher than expected, showing that the corruptions, individually, affected a larger area. Despite this, it was not possible to establish a direct relationship between the extension magnitude of corroded regions and the elevation profile along the length of the pipeline.

Figure 8 shows that in section 1, the corroded regions are more evenly distributed along the circumference of the pipe at the beginning; as the distance increases, these regions are concentrated around the 3:00 and 9:00 o'clock axes. This happens until approximately km 135, and from then on, the corroded regions become more evenly distributed. The uniform distribution at the beginning of the section can be explained by the large availability of oxygen in the period that the pipeline was in operation. The apparent decrease in density of the corroded regions at the 6 o'clock position is caused by the abrasive action of the slurry in that position. Thus, the erosive process is predominant in relation to the corrosive process.

The results of the corrosion rates presented in Figure 9 shows that the corrosion rates are higher at the beginning of

a certain pattern of concentration of corroded regions was observed at bottom points of the elevation profile in certain sections of the pipe. Regarding the distributions of the corroded regions along the pipe circumference, at the beginning of the sections, they were uniform and as the distance from the beginning increased, these corroded regions tended to concentrate around the 3 and 9 o'clock axes. The decrease in density of the corroded regions at the 6 o'clock position is caused by the abrasive action of the slurry in that position. Thus, the erosive process is predominant in relation to the corrosive process.

The characterization of the corrosion product by microstructural analysis, with the support of chemical and mineralogical analyses by X-ray

the sections, after the pumping stations at km 0 and km 153, but decreasing along the stretch, showing that the corrosive process is mainly related to oxygen dissolved in the water pumped during the operational phase. At the beginning, the rate is higher and as oxygen is consumed along the pipe, the rates showing a downward trend. This downward trend is more pronounced in the stretch between km 153 and km 274, compared to the stretch between km 0 and km 153.

Analyzing the erosion results, shown in Figure 10, it is observed that the erosion rates are higher at the beginning of the sections, km 0 and km 153, showing a downward trend along the stretch. The rates are considerably higher at the beginning of section 2 (km 153) until close to km 183. In this section, during the operational phase, the largest head losses of the system were recorded, which cause a reduction in the flow rates in the discharge of the pump station located at km 153, since the system is limited in the discharge pressure of the pumps. Thus, the minimum deposit velocity may not be reached, particle deposition may occur and the formation of beds at the bottom of the pipe will be more accentuated. If fixed beds are formed, corrosion may occur under the deposits and, if they are mobile, the erosion process will be favored. This situation could explain the higher erosion rates in this stretch. Another important point regarding the beginning of the sections is the synergistic effect of the corrosive and erosive processes.

diffraction, presents magnetite as the predominant phase, with botryoidal morphology. This magnetite is formed by the oxidation of steel of the pipeline; it should be noted that the natural magnetite, that is, originally present in the transported concentrates, is quite low; thus, almost all the magnetite analyzed comes from corrosion.

The tubercles removed from the inside of the pipeline are composed essentially of corrosion products of steel and include varying amounts of fine ore and generally very fine calcite, derived from the carbonation of calcium hydroxide used in the process.

To ensure quality and efficiency in the application of the nitrogen hibernation process, more monitoring points of the parameters along the pipeline must be

defined, in addition to the points located at the ends of the stretches. Acceptance criteria should also be established that consider the moisture values measured directly inside the duct. The possibility of reaching the nitrogen hibernation criteria at the monitoring points was observed, but due to the long distance between these points, pockets of moisture may have been trapped in the pipeline and the parameters were lost very quickly, requiring a gas exchange.

References

- AGUIRRE, J.; WALCZAK, M. Multifactorial study of erosion-corrosion wear of a X65 steel by slurry of simulated copper tailing. *Tribology International*, v. 126, p. 177-185, 2018. <https://DOI.org/10.1016/j.triboint.2018.04.029>
- ASSOCIAÇÃO BRASILEIRA DE NORMAS TÉCNICAS. *ABNT NBR 15280-2: onshore pipeline, parte 2: construction and installation*. 2015. 96 p. ISBN 978-85-07-05935-6.
- DÍAZ-DAMACILLO, L.; PLASCENCIA, G. A new six parameter model to estimate the friction factor. *American Institute of Chemical Engineers Journal*, v. 65, p. 1144-1148, 2019. DOI:10.1002/aic.16535
- ELEMUREN, R.; EVITTS, R.; OGUOCHA, I.; KENNEL, G.; GERSPACHER, B. R.; ODESHIA, A. Slurry erosion-corrosion of 90° AISI 1018 steel elbow in saturated potash brine containing abrasive silica particles. *Wear*, v. 410-411, p. 149-155, 2018. <https://DOI.org/10.1016/j.wear.2018.06.010>
- ISLAM, Md. A.; FARHAT, Z. N. Erosion-corrosion mechanism and comparison of erosion-corrosion performance of API steels. *Wear*, v. 376-377, p. 533-541, 2017. <http://dx.DOI.org/10.1016/j.wear.2016.12.058>
- LINS, V. F. C.; LAGE, F. C.; CASTRO, M. M. R.; COSTA, C. G. F.; MATENCIO, T. Strategies for corrosion inhibition of slurry pipelines prior to commissioning. *REM - International Engineering Journal*, v. 69, n. 2, p. 161-166, 2016. <http://dx.DOI.org/10.1590/0370-44672015690084>.
- LIU, A.; CHEN, K.; HUANG, X.; CHEN, J.; JIANFENG ZHOU, J.; XU, W. Corrosion failure probability analysis of buried gas pipelines based on subset simulation. *Journal of Loss Prevention in the Process Industries*, v. 57, p. 25-33, 2019.
- LIU, B.; SUN, M.; LU, F.; DU, C.; LI, X. Study of biofilm-influenced corrosion on X80 pipeline steel by a nitrate-reducing bacterium, *Bacillus cereus*, in artificial Beijing soil. *Colloids and Surfaces B: biointerfaces*, v. 197, 111356, 2021.
- MATTIOLI, G. G.; MARTINS, A. F.; LINS, V. F. C.; BRANDÃO, P. R. G.; TORRES, A. S. G. Evaluation of internal corrosion in a Brazilian iron ore slurry pipeline based on the characterization of scales and tubercles. *REM - International Engineering Journal*, v.71, n. 2, p. 203-208, 2018. <http://dx.DOI.org/10.1590/0370-44672017710073>
- PENG, X.; HUANG, Z.; CHEN, B.; LIU, D.; LI, H. On the interference mechanism of stray current generated by DC tram on pipeline corrosion. *Engineering Failure Analysis*, v. 116, 104760, 2020.
- TAYLOR, J. B.; CARRANO, A. L.; KANDLIKAR, S. G. Characterization of the effect of surface roughness and texture on fluid flow-past, present, and future. *International Journal of Thermal Sciences*, v. 45, p. 962-968, 2006. DOI:10.1016/j.ijthermalsci.2006.01.004

Received: 9 February 2021 - Accepted: 6 February 2024.